Scholar Publishing Group
International Journal of Neural Network
https://doi.org/10.38007/NN.2022.030101
ISSN 2790-2692 Vol. 3, Issue 1: 1-14

A Non-contact VR Video Image Measuring System for Cell Strain Measurement and Mechanical Performance Characterization

Tingjun Guo*

Jilin International Studies University, Jilin, China

**corresponding author*

Keywords: Image Measurement System, Cell Strain Measurement, Biomechanics, Non-contact VR Image Measurement

Abstract: VR panorama, or virtual reality, has become a new medium for mass media. Its collection of special technical hardware including computers, head-mounted displays, headphones, and motion-sensitive gloves has been widely used in various fields. The purpose of this article is to study a non-contact VR video image measurement system that can be used for cell strain measurement and mechanical property characterization. In this paper, through the extraction of cell feature points, as well as cell morphology processing and image graying, etc. The observed static cells exhibit dynamics. Under the example test of the protein elastic deformation measurement experiment in the cell nucleus and the mechanical characterization experiment of the cell hardness measurement, it is concluded that the percentage of the volume strain change of the cell is about The result of the shear strain change percentage is about 4 times, and the maximum relative error of the image measurement system is 2.36%, which indicates that the measurement of the VR video image measurement system in this paper is feasible and effective. It better solves the shortcomings of current cell observation and measurement, and can be applied to modern biological development or medical research with more excellent technology.

1. Introduction

In recent years, with the vigorous development of society and science and technology, VR technology has also developed to a certain stage. People's demand for him also increased, and slowly became a new technological direction. With the rapid development of image processing technology at home and abroad, some researchers began to study some identification and feature parameter extraction techniques for tiny biological cells, and achieved some good results. Non-contact VR video image measurement technology is highly regarded by many entrepreneurs

and scholars because it is relatively fast and convenient.

VR video image vision is the main link between intelligent manufacturing and computer science development and progress. Safety inspections, microscope images, aerospace measurement and mapping, medical assistance, scientific exploration, etc., have a variety of detection situations in industry, medical care, and military directions. The broad application algorithm is also an important link to realize intelligent manufacturing and industry [1]. The new technology field formed after the introduction of the machine vision system has vision measurement technology. The main research objectives are to measure important parameters of the object, batch inspection of the workpiece, and crack indentation detection. This non-contact measurement is an advantage that can meet the measurement requirements of accuracy, speed, and stability. The visual measurement technology is effective, and it is also an effective reason for frequent use in more and more industries and fields.

Zhang Y proposed an improved Φ-OTDR system based on ultra-weak fiber Bragg grating array, which can use narrow pulses to achieve quantitative strain measurement, which can extend the detectable fiber length. His experimental results show that a quantitative strain measurement at the end of a 4km long sensing fiber can be achieved with a 50ns pulse [2]. Shao X believes that due to the influence of out-of-plane motion, the accuracy of strain measurement using a general optical extensometer with two-dimensional (2D) digital image correlation (DIC) is not sufficient for experimental applications. Although a three-dimensional (3D) DIC can measure all three components of displacement without introducing in-plane displacement errors, 3D-DIC requires strict synchronization between the two digital cameras and requires complex binocular stereo vision system calibration , Which makes the measurement quite inconvenient. In order to solve the above problems, he proposed a self-calibrating single-lens 3D video extensometer for non-contact, non-destructive and high-precision strain measurement. In the video extensometer he built, a single-lens 3D imaging system with a prism and two mirrors was constructed to obtain a stereoscopic image of the test sample surface, so the problems of synchronization and out-of-plane displacement can be easily solved [3]. Pan B has developed an advanced video extensometer for non-contact, real-time, high-precision strain measurement in material testing. In the established video extensometer, he constructed an "nearly perfect and ultra-stable" imaging system, combining the idea of active imaging with high-quality bilateral telecentric lenses to obtain high-fidelity video images on the surface of test samples. Therefore, it does not change with the change of the ambient light, and a small out-of-plane motion occurs between the surface of the object and the image plane. In addition, he adopts an efficient and accurate inverse combined Gauss-Newton inverse algorithm, which combines time initial guess transfer scheme and high-precision interpolation method to achieve real-time, high-precision displacement tracking with negligible displacement error. Tensile tests were performed on aluminum samples and carbon fiber wire samples to prove the efficiency, repeatability and accuracy of the developed advanced video extensometer. His results indicate that longitudinal and lateral strains can be estimated and plotted at a rate of 117 fps, and are maximum [4].

In this paper, through the introduction of non-contact measurement technology and VR three-dimensional panoramic measurement technology and biomechanics, and through the processing of distorted image morphology and image graying algorithm, combined with three-dimensional VR technology, strain measurement of hamster cells in the experiment Observe the characterization of the mechanical properties of its cells, and express the results by analyzing the error of the results in the experiment and the degree of observation of the cells by comparing the experimental results with traditional observation and measurement methods. And through the results of the relationship between the volumetric strain of the cells and the pressure, we can see the

feasibility and effectiveness of the VR video image measurement system in this paper.

2. Proposed Method

2.1. Non-contact Image Measurement Technology

The non-contact VR video image measurement technology makes up for the shortcomings of traditional measurement and obtains more accurate and standard results. Use the image information of the measured object as a carrier for detection and transmission [5-6] to extract useful information from the image. Non-contact measurement methods can be divided into three-dimensional VR measurement in space and two-dimensional pattern measurement [7-8].

2.2. VR Three-dimensional Measurement Technology

VR video image measurement technology includes lattice method, optics, camera method, scanning method, mechanical and electrical methods. The camera method has undergone excessive development from two-dimensional cameras to three-dimensional cameras [9-10]. The two-dimensional camera method captures the instantaneous movements of human motion, and measures and discusses the images. Although subject to the shadow distance limitation of the projection and the change of the phase difference, the shooting distance is generally less than 9m, so the shooting is performed at a ratio of 1/10. In the three-dimensional camera method, the principle of binocular imaging in the computer observation system is used. Using a camera, you can obtain a two-dimensional picture of a three-dimensional pattern, that is, a two-dimensional picture between the coordinates of the real space and the plane coordinate system of the camera image, extract an index that can express the pattern very much, and synthesize the characteristic lines of the human body (vertical gaps, etc.) As the line level, as the line of the three-dimensional coordinate diagonal). When the image is still, the TV camera will capture the light he projects. The shape of the pattern is represented by a series of cross-sections, resulting in a three-dimensional surface shape [11-12].

There are two basic scanning methods: laser scanning and infrared scanning. Using several lasers to receive the reflected light from the pattern surface in all directions is a laser scanning method. The coordinates of the same height of the image are calculated based on the light receiving location, optical axis angle, and gap, and all the data of the cell pattern surface are obtained [13-14]. Using the camera to capture the appearance of the pattern and the shape of the picture is an infrared scan. The crossed arms are automatically controlled and move back and forth from top to bottom. The sensor repeatedly scans the entire pattern on the cross arm. The computer first processes the obtained outline size, obtains the frame model of the shape, then solves the number of the thermal image measured by the sensor, modifies the frame model of the image, and completes the overall measurement "Mohr method, duplication method, position method". This is the principle of the lattice. Through optical measurement, the shadow of the lattice and the outline of the moir é fringe are formed, and the shape information such as the unevenness of the body surface, the cross section, and the development of the scale can be obtained [15-16].

2.3. Feature Point Extraction

(1) Distorted image morphology processing

For the extraction of cross feature points in the image, in order to accurately extract the pixel coordinate points, it is necessary to perform preprocessing operations on the distorted image. First,

the binarized processing is performed on the distorted image of the leaf with a grid background, which simplifies the post-processing and improves Calculate the speed, through the proportion of the size of the calibration plate that the blade object occupies, you can predict the proportion of the blade object to the entire image, and select the P parameter method to select the threshold. The specific steps are as follows: predict the image proportion of the object and record it as P The target blade object is dark, and the background is relatively bright. Calculate the histogram distribution P (t) of the image, let t = 0,1 ..., 255, calculate the threshold T, so that T can meet the minimum value in the formula, choose the appropriate The threshold T will transform the image into a binary image [17-18].

$$P^{'} = \left| \sum_{t=0}^{T} P(t)/m \cdot n - P \right| \tag{1}$$

Two basic operations of morphology: corrosion and dilation. Corrosion can make the target area smaller. Its essence is to reduce the boundary of the target image. The structure pixel object used for corrosion dilation and other operations is called the structure element. The structure pixel B When scanning step by step and shifting by distance a, it can be written as, if it is included in the image X, the formula can be expressed as [19-20]:

$$E(X) = \left\{ a \middle| B(a) \subset X \right\} \tag{2}$$

The expansion operation in mathematical morphology can be expressed as:

$$E(Y) = \left\{ y \middle| B(y) \mathrm{I}\ Y \neq \phi \right\} \tag{3}$$

This operation first performs a convolution operation on the structural element B on the image, similar to the scanning and translation process in the erosion operation. In the scanning process of the structural element, if there is an intersection between the sub image covered by the call and the The value of the position corresponding to B in the result image is set to 1, otherwise it is set to 0.

(2) Grayscale image

Color is our perception of light of various frequencies reaching the retina. Our method of describing color is generally measured by three different quantities. The three-dimensional space coordinates can be formed by three variables, which is the color space. If colors are described at different angles and different attributes, different color spaces will be created. In color theory, the most common colors can be expressed by mixing three basic colors of red (R), green (G), and blue (B), so in a color image, the color of each pixel of the image is R, G And three components. The value range of each component is: R: 0.255, G: 0.255, B: 0.255. The process of processing a color image into a grayscale image is called image grayscale calculation. The amount of image processing calculation after image grayscale processing is relatively reduced, and R, G, and B components of the color image are extracted from the corrected image. In order to promote the human visual system, the color processing space used in image processing is the HSI color space. Both HSI and RGB can be used to represent the color space, only that the components are different, and both can be converted to each other [21-22]:

$$H = \begin{cases} \theta, G \geq B \\ 2\pi - \theta, G < B \end{cases} \tag{4}$$

$$\theta = \arccos\left\{\frac{(R-G)+(R+B)}{2\sqrt{(R-G)^2+(R+B)(G-B)}}-\right\} \tag{5}$$

$$S = 1-\frac{3\min(G,R,B)}{R+G+B} \tag{6}$$

$$I = \frac{1}{3}(R+G+B) \tag{7}$$

I In equation (7), the gray value (luminance value), that is, the three components of R, G, and B, and the parameter values of R, G, and B are combined to calculate the gray image value. The range can be obtained from the gray range of 0 to 255. By performing gradation processing on the image, the amount of image processing calculation can be reduced. It can also prepare for subsequent operations such as image segmentation and image recognition. Common graying processing methods are as follows:

1) Maximum method

This method takes the largest gray value among the three components of ruler, G, and B. At this time, the gray value of this component is used as the gray value in the graying operation of the image. The formula can be expressed as:

$$f(i,j) = \max\left(R(i,j), G(i,j), B(i,j)\right) \tag{8}$$

2) Average method

For the three components in the color image, the gray values are added and averaged. At this time, the gray value can be expressed as the gray value in the graying operation of the image by the formula:

$$f(i,j) = \left(R(i,j)+G(i,j)+B(i,j)\right)/3 \tag{9}$$

3) Weighted average method

The three components are weighted and averaged in different proportions. In the human visual system, among the three colors of R, G, and B, we are more sensitive to green G, followed by R, and weaker to blue B. Therefore, according to different weights, when the components are $G(i,j) > R(i,j) > B(i,j)$, the calculation of the three components of R, G, and B according to formula (10) is more suitable for the grayscale image of human vision [23-24]:

$$f(i,j) = 0.30R(i,j)+0.59G(i,j)+0.11B(i,j) \tag{10}$$

2.4. Methods of Measuring Intracellular Strain:

(1) Use photo processing guidelines to detect cell edge contours.

(2) Use a computer to open the operation to obtain the cell morphology.

(3) Split the internal structure of the biological cell area [25-26].

(4) Through the analysis of the electric field magnetic field and mechanical effects, construct a method for measuring intracellular strain.

3. Experiments

3.1. Measurement Experiment of Protein Elastic Deformation in the Nucleus

(1) Experimental materials and methods

Experimental materials: laser confocal microscope, three-dimensional magnetic distortion system, vertical mixer, desktop low-speed centrifuge, ultra-pure water meter, waste tank, petri dish, DMEM high glucose liquid medium, PBS phosphate buffer, cell culture DMSO dimethyl sulfoxide, TrypLE, fetal bovine serum, type I collagen, L-glutamic acid, Arg-Gly-Asp, sodium pyruvate, etc.

Culture method: Most hamster ovary cells (CHO) have a division cycle of around 22h to 28h. Usually need to conduct an agent every 3 days. Whenever inheritance is carried out, it is necessary to determine the inheritance rate through the required amount of experiments. About 22% is enough. He is a somatic cell, and CHO cells are preserved. First, a CHO cell culture site is constructed according to a specific ratio. According to the experimental plan, 49ml of PBS phosphate buffer (1X) was added to 498ml of Ham's F12 nutrient-requiring medium. Then add 5 ml of cell culture double antibody.

(2) VR image acquisition operation steps

1) At the beginning, the temperature must be kept at 25 ℃. Before preparing for the experiment, the air conditioner must be turned on. A stable and reliable temperature is the basis for maintaining the experiment.

2) Power on the computer, STED microscope, and VR video imaging equipment.

3) Embed the end plate of the experiment into the hole of the VR video image on the stage of the STED microscope, and keep it horizontal to avoid tipping.

4) Open the application software system on the computer, mainly based on the reliable data required by the experiment, including the frequency, stage, and number of cycles of the post-burner.

5) Use a VR video imaging system to generate a 500ms pulse to magnetize the magnetic ball coated on the cell surface. The intensity of the generated magnetic field is about 2400 Gauss / ms, and the magnetization is 2-4 times.

6) Then, when the platform is stable, perform the measurement without force, use the external synchronization trigger button to control the microscope synchronous operation, and obtain the image without force and leave it.

7) Then conduct the post-combustion experiment, design through the software system on the computer, use the external synchronous trigger mode to control the microscope synchronously, obtain the image and save the combustion image.

8) Use Matlab software's magnetic ball tracking program to process the collected images, and output the table values through calculation including the sampling frequency and magnetic ball motion coordinate values.

9) Remove the abnormal motion value of the magnetic ball, and finally calculate the hardness of the cell.

The experiment measured the deformation of the protein in the nucleus under various directions (0 °, 45 °, 90 °). The observed elastic deformation mainly includes cutting changes, posture changes, and spontaneous rotation. First, according to the method used in the cell hardness measurement experiment, the initial image was collected under various conditions, the image was modified, imported into the system's software, and the calculation application output the elastic deformation of the nuclear protein after a specific torque.

3.2. Mechanical Characterization Experiment of Cell Hardness Measurement

When a 4.5-micron-diameter magnetic ball coated with a specific protein is attached to the cell surface, the magnetic ball will bind to the cell's receptor and cell skeleton to form an attachment point. The detailed key steps of the cell hardness determination experiment are as follows.

(1) First, when the magnetic ball is magnetized along the Z-axis direction perpendicular to the cell plane, the magnetic ball generates magnetization M perpendicular to the cell plane direction.

(2) Apply the external magnetic field of the sine wave to the magnetic ball at a specific angle (0 ° or 90 °). The vector product of the magnetic induction H, M, H is equal to the magnitude of the sinusoidal moment T applied to the cell. Due to the different orientation of the force, according to the generated sinusoidal torque T, the cells can be twisted and moved to different positions at the same time.

(3) Run a super-resolution microscope to collect and record patterns, and then perform image-related processing, including image noise reduction, image generation, merge patterns, format changes, analysis of edges, etc.

(4) Input the processed image into the VR software program, and calculate the displacement of the cell through the system. Then, according to the calculation method and formula.

To achieve the measurement requirements of the cell hardness based on the VR panoramic video image measurement system and the microscope cell biomechanics system, relevant experiments will be designed according to the above experimental methods to realize the observation of the cell hardness. If the frequency of the torsional magnetic field is 2 Hz, the measurement results of the cell hardness are calculated under two forces applied in different directions (0 °and 90 °). Under the condition of a torsion magnetic field frequency of 2 Hz, the force is 20 Pa, observe the movement of the magnetic ball in the direction of 0 °and 90 °, and calculate the values in two different directions (0 °and 90 °).

4. Discussion

4.1. Analysis of the Experimental Results of Protein Elastic Deformation Measurement in the Nucleus

The magnetic balls left in the initial solution were mixed and pulverized, and after shaking for 4 minutes with an ultrasonic oscillator, 100 mL was sucked in using a pipette and added to a remote sink tube (1.5 ml). After that, centrifugation was performed at a speed of 1400 rpm and a centrifuge time of 6 minutes. The cells were then washed, sucked up with a pipette, and then discarded into a waste tank. As shown in Table 1, without drawing cells from the bottom of the centrifuge tube, PBS solution (10 mL) and RGD solution (1 ml) were added to the centrifuge tube.

Table 1. Usage of PBS and RGD in experimental mice at various ages

Week	12W	16W	22W	28W	36W	45W	66W	75-84W
PBS(ml)	10	10	7	13	5	13	8	10
RGD(μ m)	5	7	4	8	3	6	9	5

Table 1 shows the usage of PBS and RGD in experimental mice at various weeks of age. The cell experiment methods and steps mainly include the cultivation of mouse melanoma cells and the

recovery of frozen cells. In the experiment, the displacement and strain diagram of the cell can be observed when the force is not applied, as shown in Figure 1 below.

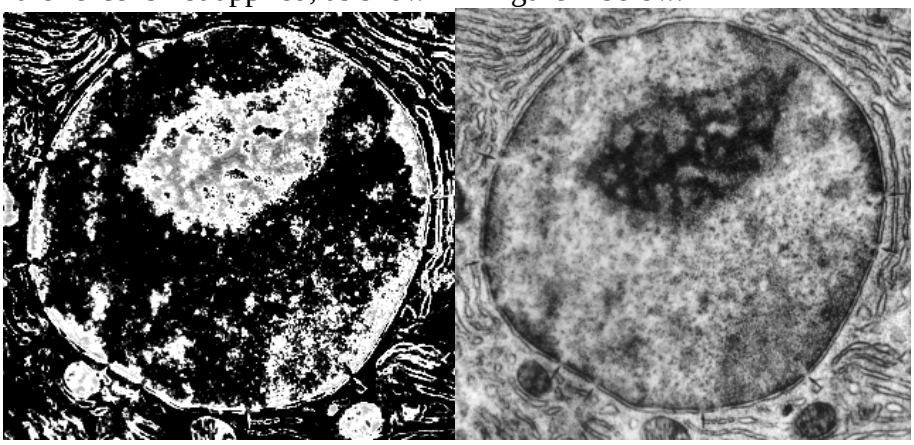

(a) *(b)*

Figure 1. Displacement and strain diagram of cells without force.

Figure 1 is a graph of displacement changes (a). The scale on the right column indicates the size of cell displacement. The scale of the right column of the shear strain diagram (b) indicates the magnitude of the cell strain. The volume strain diagram and the scale in the sidebar indicate the size of the cell volume strain. The ratio in the right-hand column of the redirection indicates the magnitude of the change in cell rotation.

By comparing the forcing forces in the above directions, it can be concluded that under the condition of the forcing force in the same direction (20 Pa), the rate of change of the volumetric strain of the cell is almost equal to the rate of change of the shape strain. About 4 times, the rigid rotation ratio of the cell is about 80% of the shear strain. Under the same conditions of the applied force (20 Pa), in the process of increasing the direction of the applied force from 0 ° to 90 °, the percentage of the body's postural distortion changes, the percentage of the shear strain changes, and the unit's The percentage of rigid rotation changes will increase gradually as the angle of post-conversion becomes larger. When the forced angle is 0 °, the change in distortion is minimal. When the forced angle is 90 °, the distortion is maximum. When the forced angle is 45 °, the distortion changes between the forced angle of 0 °. 90 ° in the middle. In addition, the difference between volume strain and shear strain caused by different directions of force is related to the percentage change of histogram displacement in the core.

Therefore, the combination of three-dimensional panoramic image measurement and nanometer-range video image measurement system can systematically provide accurate discussions and algorithms of protein deformations that constitute the nucleus, and also constitute specifications for scientific measurement methods that have specific effects on shape and function.

4.2. Experimental Analysis of Mechanical Characterization of Cell Hardness Measurement

When the frequency of the torsional magnetic field is 0.4 Hz, when the force is applied in 3 different directions (0 °, 45 °, 90 °), when the force is applied in the 0 ° direction (the direction of the force is parallel to the long axis direction of the battery), the battery When the stretch is the smallest, the cell hardness is the largest. The direction of 90 ° (the direction of force) is upward and

perpendicular to the long axis direction of the cell, with the greatest degree of extension and the smallest cell stiffness; if the frequency of the torsional magnetic field is 1 Hz, it is directed in 3 different directions (0 °, 45 °, 90 °) The applied force is the same as at 0.3 Hz, but when the angle of the force is the same, the frequency of the torsional magnetic field is 1 Hz. The details are shown in Figure 2 below.

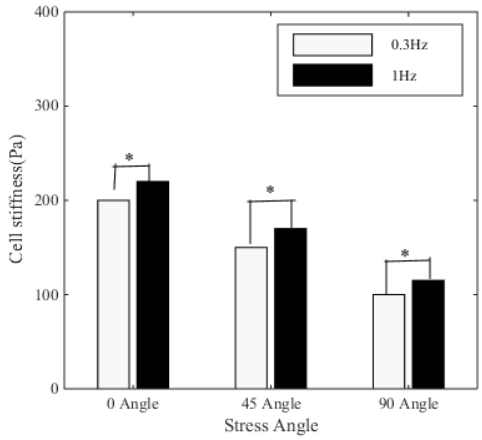

Figure 2. Cell hardness when force is applied in different directions

Figure 2 shows the rigidity of the unit when force is applied in different directions. The histogram on the left shows the power of 15 Pa at 0.3 Hz and cell hardness in all directions, and shows the power of 15 Pa at 1 Hz and cell hardness in all directions. There is a significant difference between the two, * means P <0.05. The cell hardness is 0 °maximum 90 °minimum, showing the mechanical mutual exclusion of the cells. As the frequency of force increases, the hardness of the cell increases, showing the viscoelastic properties of the cell. 10 independent experimental tests were conducted on a total of 10 groups of cells at two frequencies (0.3 Hz and 1 Hz). The results are shown in Figure 3.

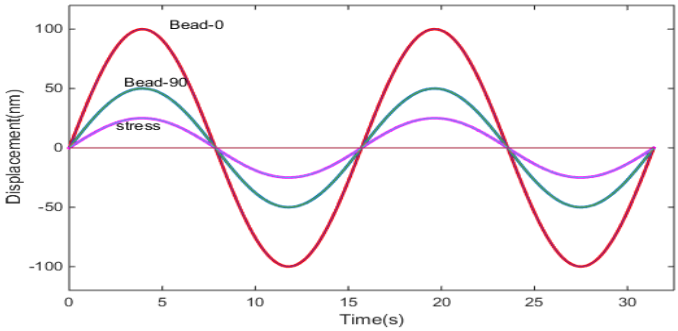

Figure 3. Cell hardness in different directions

Figure 3 is a sine function image of the magnetic ball and the torsion force of the magnetic ball displacement tracking. Displacement is the average of 7 cycles used to remove noise. Displacement and force are synchronized, but due to the viscoelasticity of the two units, there is a slight delay.

The experimental results of cell hardness measurement show that the size of the cell hardness is greatly affected by the forced angle change. The magnitude of the force is unchanged. If the frequency of the torsion magnetic field is the same, the angle of the force increases from 0 °to 45 °,

and finally increases to 90 °, and the hardness of the cells will gradually decrease. This result is consistent with the long axis direction of the microfibers constituting the intracellular skeletal myocardium, and it is confirmed that the cell hardness is closely related to the long axis direction of the microfibers. This is because the cytoskeletal acrylic acid inside the cells constitutes a bundle of microfibers. When the direction of the force is perpendicular to the long axis direction of the microfiber bundle (90 °), because the rope will be tightened, according to this stretching, it will produce large vibration and displacement; therefore, the frequency and force of the twisted magnetic field Under the condition of the same size, if the angle of force is perpendicular to the long axis of the tow, the hardness of the unit will be the smallest. In addition, when the angle of force is small, if the long axis of the rattan is parallel, the hardness of the cell is the largest.

Therefore, the cell biomechanics research platform combined with the nano-microscope based on VR technology can quickly measure the hardness of the cell at a single frequency or multiple frequencies, and realize the quantitative measurement of the mandatory impact on a single cell. At the same time, you can also use a research platform to force cells for a long time at a specific frequency to observe and measure the real-time changes in cell hardness caused by changes in cell skeleton structure and cell contractility.

4.3. System Feasibility Analysis

Test and evaluate the feasibility of the non-contact VR video image measurement system, which can be reflected by the system measurement error. The smaller the measurement error is, the higher the system accuracy is. The measurement result can be used to judge whether the system has reached the expected target.

The following will use the traditional measurement method and the VR technology processing method in this paper. The experimental materials are selected to be 5 universally known shapes that are close to the shape of the blade: rectangle, ellipse, diamond, pentagonal star and regular pentagon, the graphic label is Al, A2, ⋯, A5, using the grid method in the traditional measurement method and the weighing method in the modern measurement method and the VR-based image measurement system method established in this paper, taking the rectangular A1 as an example, the original image and measurement results are shown in the figure As shown below, multiple experiments and data analysis were performed on the measurement accuracy index of each method. The coefficient of variation of the measurement results of each method was analyzed through multiple measurements to evaluate the stability of the system. The measurement results are shown in Table 2 below.

Table 2. Measurement results of different measurement methods

Image	Area	Traditional measurement method		Modern surveying		VR Measurement	
		Area(cm^2)	Error	Area(cm^2)	Error	Area(cm^2)	Error
A_1	50.27	51.30	2.05%	51.54	2.53%	49.26	2.00%
A_2	27.52	28.06	1.96%	28.25	2.65%	27.05	1.72%
A_3	28.00	28.74	2.64%	28.75	2.67%	27.42	2.06%
A_4	21.27	21.37	2.18%	21.89	2.91%	20.93	2.36%
A_5	64.50	66.00	2.33%	65.88	2.14%	63.35	1.79%

From the measurement results in Table 2, it can be shown that the area values of the objects measured by the three measurement methods are not much different, and there is a significant correlation between the three methods. The relative error of the measurement results of the traditional measurement method is small, which can be used as the subsequent leaf area The accuracy comparison method in the measurement experiment, in which the relative error of the area measured by the modern measurement method and the VR video image measurement system is relatively small, and the measurement result is more accurate. From the table, it can be concluded that the maximum relative error of the VR video image measurement system is Within 2.36%, the average measurement accuracy of the system is ± 1.99%, which is better than traditional manual measurement methods and modern measurement methods, and meets the actual measurement requirements. The specific situation is as shown below.

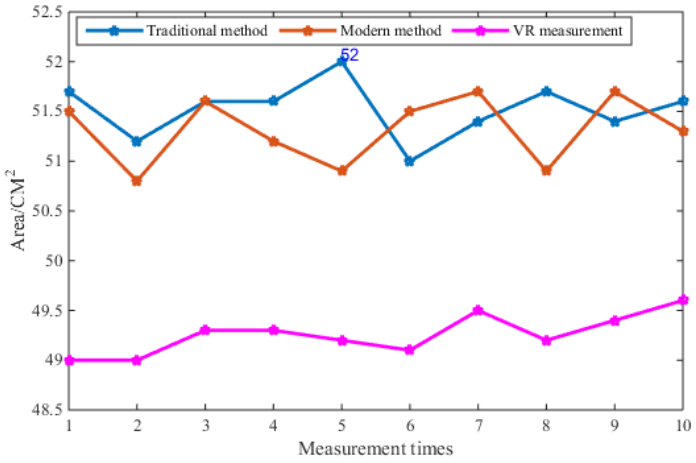

Figure 4. Change graph of measurement results

The change curve of the measurement result is shown in Figure 4. As can be seen from the figure, due to the different placement of objects in each image area measurement by the traditional method, there is a deviation in the total number of grids each time, and the area measurement results vary greatly , The coefficient of variation reaches 0.70%, indicating that the traditional method of measurement results are relatively unstable, the curve of the modern measurement method and the VR video image measurement system used in this article changes relatively smoothly, the coefficients of variation are 0.61% and 0.46%, respectively. Smaller, better stability of measurement results. In summary, the measurement results of the measurement system in this paper are more accurate and the measurement results are more stable. The measurement of the VR video image measurement system is feasible and effective.

5. Conclusion

VR technology realizes a profound observation effect from the human point of view to small cell morphology, obtains observation effects in all ranges, confirms the real-time interaction and real-time dynamic situation, and can concentrate on the surrounding environment. As the main application link of intelligent manufacturing and machine vision, vision measurement technology is used in precision measurement and control, computer technology, optoelectronics technology and other fields [27]. The development and development of the actual working conditions of visual measurement systems are more complicated.

This paper uses cell biomechanical analysis based on the combination of VR three-dimensional video image measurement system to analyze the results of cell hardness measurement experiments, showing the results of cell hardness measurement and nuclear protein displacement measurement. Second, the elastic deformation of proteins in the core includes changes in shear strain, volume strain, and rigid rotation. According to these experimental results, the experimental results show that the non-contact VR image measurement system provides a synchronized real-time, high-resolution, accurate and convenient observation method to measure the mechanical properties of cells.

The dynamic images of small cells and the feature size of cells are connected through a computer network. To achieve effective measurement of cell mechanical properties. This helps to resolve the contradiction between evolving microbiology and inadequate images. The proposed image algorithm is suitable for VR image measurement systems. Tool parameters are collected under online and offline measurement status. The collected images use traditional algorithms and the algorithm in this paper for experimental simulation. The effectiveness of the proposed algorithm will be verified in the VR image measurement system.

Funding

This article is not supported by any foundation.

Data Availability

Data sharing is not applicable to this article as no new data were created or analysed in this study.

Conflict of Interest

The author states that this article has no conflict of interest.

References

[1] Lv, Zhihan, et al. "Digital Twins Based VR Simulation for Accident Prevention of Intelligent Vehicle." IEEE Transactions on Vehicular Technology (2022). https://doi.org/10.1109/TVT.2022.3152597

[2]Zhang Y, Guo Z, Qiao W, et al. Improved Φ-OTDR system with narrow pulses for quantitative strain measurement based on ultra-weak fiber bragg grating array. Microwave & Optical Technology Letters, 2016, 58(12):2892-2894. https://doi.org/10.1002/mop.30178

[3] Shao X , Eisa M M , Chen Z , et al. Self-calibration single-lens 3D video extensometer for high-accuracy and real-time strain measurement. Optics Express, 2016, 24(26):30124. https://doi.org/10.1364/OE.24.030124

[4] Pan B , Tian L . Advanced video extensometer for non-contact, real-time, high-accuracy strain measurement. Optics Express, 2016, 24(17):19082-19093. https://doi.org/10.1364/OE.24.019082

[5] Vrana, Branislav, Vermeirssen, E. L.M, Allan, I.J. Passive sampling of emerging pollutants in the aquatic environment: state of the art and perspectives. Position Paper. Journal of Combinatorial Theory, 2016, 113(8):1621-1628.

[6] Hasegawa M , Mori M , Matsumura J . Non-Contact Velocity Measurement of Japanese Cedar Columns Using Air-Coupled Ultrasonics. World Journal of Engineering & Technology, 2016,

04(1):45-50. https://doi.org/10.4236/wjet.2016.41005

[7] Vrachimis S G , Eliades D G , Polycarpou M M . Real-time hydraulic interval state estimation for water transport networks: A case study. Drinking Water Engineering and ence, 2018, 11(1):19-24. https://doi.org/10.5194/dwes-11-19-2018

[8] Ho C C , Chang Y J , Hsu J C , et al. Residual Strain Measurement Using Wire EDM and DIC in Aluminum. inventions, 2016, 1(1):4. https://doi.org/10.3390/inventions1010004

[9] Romao-Veiga M , Ribeiro V R , Romagnoli G G , et al. 42 MSU involvement in adaptive immunity activation in PBMCS from pregnant women with preeclampsia. Pregnancy Hypertension, 2016, 6(3):197-198. https://doi.org/10.1016/j.preghy.2016.08.124

[10] Shafiei S , Dabbagh V R , Sadra H , et al. The comparison between ultrasonography and 99mTc-DMSA Renal scan in estimation of kidney size. Iranian Journal of Nuclear Medicine, 2016, 24(1):23-28.

[11] Turnbull A E , Rabiee A , Davis W E , et al. Outcome Measurement in ICU Survivorship Research From 1970 to 2013: A Scoping Review of 425 Publications. Critical care medicine, 2016, 44(7):1267. https://doi.org/10.1097/CCM.0000000000001651

[12] Okay Abaci, Cuneyt Kocas, Veysel Oktay. Relationship between myocardial performance index and severity of coronary artery disease in patients with non-ST -segment elevation acute coronary syndrome : Cardiovascular topics. cardiovascular journal of africa, 2017, 28(1):4-7. https://doi.org/10.5830/CVJA-2016-041

[13] Driver VR, Reyzelman A, Kawalec J. A Prospective, Randomized, Blinded, Controlled Trial Comparing Transdermal Continuous Oxygen Delivery to Moist Wound Therapy for the Treatment of Diabetic Foot Ulcers.. ostomy/wound management, 2017, 63(4):12.

[14] Vijay Reddy Venumuddala, Sridhar Moturi, S V Satish. Endodontic Management of a Maxillary First Molar with Seven Root Canal Systems Evaluated Using Cone-Beam Computed Tomography Scanning.. journal of international society of preventive & community dentistry, 2017, 7(5):297-300.

[15] Jiang T, Bai L, Yuan H, et al. A Novel QV Interaction Evaluation and Pilot Voltage-Reactive Power Coupling Area Partitioning in Bulk Power Systems. Iet Science Measurement Technology, 2016, 11(3):270-278. https://doi.org/10.1049/iet-smt.2016.0232

[16] Deulgaonkar V R . Vibration Measurement and Spectral Analysis of Chassis Frame Mounted Structure for Off-Road Wheeled Heavy Vehicles. International Journal of Vehicle Structures & Systems, 2016, 8(1):23-27. https://doi.org/10.4273/ijvss.8.1.05

[17] Papandreou M , Diamantis E , Vrachlioti V I , et al. Clinical evaluation of static scapular posture in overhead athletes with asymptomatic shoulder injuries. Journal of Sports Medicine & Physical Fitness, 2018, 58((7-8)): 1071-1077. https://doi.org/10.23736/S0022-4707.17.07751-9

[18] R Tudosescu, CM Alexandrescu, SL Istrate. Correlations between internal and external ocular factors and macular pigment optical density. romanian journal of ophthalmology, 2018, 62(1):42-47. https://doi.org/10.22336/rjo.2018.6

[19] Gao S , Baker C , Chen L , et al. Approach for temperature-insensitive strain measurement using a dual-core As 2 Se 3 -PMMA taper. Optics Letters, 2018, 43(7):1523. https://doi.org/10.1364/OL.43.001523

[20] Hensley S , Christensen M , Small S , et al. Digital image correlation techniques for strain measurement in a variety of biomechanical test models. Acta of Bioengineering & Biomechanics, 2017, 19(3):187-195.

[21] Song G , Sun T, Y. Lü, et al. Wireless Strain Measurement Based on a Microstrip Patch Antenna. Transactions of Nanjing University of Aeronautics & Astronautics, 2017,

34(5):477-486.

[22] Quadflieg T, Gries T, Stolyarov O. Strain measurement in concrete using embedded carbon roving-based sensors. Materialprufung, 2016, 58(9):767-771. https://doi.org/10.3139/120.110913

[23]Sitzmann V , Serrano A , Pavel A , et al. Saliency in VR: How do people explore virtual environments?. IEEE Transactions on Visualization & Computer Graphics, 2016, 24(4):1633. https://doi.org/10.1109/TVCG.2018.2793599

[24] Furukawa O , Tezuka S I , Tsukamoto M , et al. Beyond 21 km Distributed Strain Measurement with Brillouin Optical Correlation Domain Reflectometry Using Polarization Diversity Method and Temporal Gating Scheme. Ieej Transactions on Fundamentals & Materials, 2017, 137(1):52-57. https://doi.org/10.1541/ieejfms.137.52

[25] Zhou K, Liu Z, Mao Y, et al. Plane two-dimensional strain measurement method of patch antenna sensor. Yi Qi Yi Biao Xue Bao/chinese Journal of Scientific Instrument, 2018, 39(1):136-143.

[26] Reisgen U , Sharma R . In-situ Strain Measurement of Submerged Arc Welding Process Through Application of Electronic Speckle Pattern Interferometry. journal of welding & joining, 2017, 35(4):82-88. https://doi.org/10.5781/JWJ.2017.35.4.12

[27] Lv Z , Chen D , Lou R , et al. Industrial Security Solution for Virtual Reality. IEEE Internet of Things Journal, 2020, PP(99):1-1.